AD

TECHNICAL REPORT ARCCB-TR-02011

EVOLUTION OF SURFACE STRUCTURES IN SPUTTERED COATINGS

MARK A. JOHNSON
PAUL J. COTE

AUGUST 2002

US ARMY ARMAMENT RESEARCH,
DEVELOPMENT AND ENGINEERING CENTER
Close Combat Armaments Center
Benét Laboratories
Watervliet, NY 12189-4000

TACOM-ARDEC

DISCLAIMER

The findings in this report are not to be construed as an official Department of the Army position unless so designated by other authorized documents.

The use of trade name(s) and/or manufacturer(s) does not constitute an official endorsement or approval.

DESTRUCTION NOTICE

For classified documents, follow the procedures in DoD 5200.22-M, Industrial Security Manual, Section II-19, or DoD 5200.1-R, Information Security Program Regulation, Chapter IX.

For unclassified, limited documents, destroy by any method that will prevent disclosure of contents or reconstruction of the document.

For unclassified, unlimited documents, destroy when the report is no longer needed. Do not return it to the originator.

REPORT DOCUMENTATION PAGE

Form Approved
OMB No. 0704-0188

1. AGENCY USE ONLY (*Leave Blank*)	2. REPORT DATE	3. REPORT TYPE AND DATES COVERED
	August 2002	Final

4. TITLE AND SUBTITLE
EVOLUTION OF SURFACE STRUCTURES IN SPUTTERED COATINGS

5. FUNDING NUMBERS
AMCMS No. 6111.02.H671.1

6. AUTHORS
Mark A. Johnson and Paul J. Cote

7. PERFORMING ORGANIZATION NAME(S) AND ADDRESS(ES)
U.S. Army ARDEC
Benet Laboratories, AMSTA-AR-CCB-O
Watervliet, NY 12189-4000

8. PERFORMING ORGANIZATION REPORT NUMBER
ARCCB-TR-02011

9. SPONSORING / MONITORING AGENCY NAME(S) AND ADDRESS(ES)
U.S. Army ARDEC
Close Combat Armaments Center
Picatinny Arsenal, NJ 07806-5000

10. SPONSORING / MONITORING AGENCY REPORT NUMBER

11. SUPPLEMENTARY NOTES
Presented at the 6th World Multiconference on Systemics, Cybernetics, and Informatics, Orlando, FL, 14-18 July 2002.
Published in Proceedings of the IIIS World Multiconference on Image, Acoustic, Speech, and Signal Processing.

12a. DISTRIBUTION / AVAILABILITY STATEMENT
Approved for public release; distribution unlimited.

12b. DISTRIBUTION CODE

13. ABSTRACT *(Maximum 200 words)*

The evolving surface structure of sputtered tantalum and niobium coatings was characterized in terms of dynamic scaling exponents using atomic force microscopy (AFM) to map surface structures over a range of scales from 10-nm to 5-□m. New numerical techniques are introduced to systematically determine the time evolution of the spatial scaling parameters associated with the coating surface morphology. These dynamic scaling parameters define a unique *universality class* that is associated with the deposition process, and provides insight into the dynamics of the growth processes of thick metal films.

14. SUBJECT TERMS
Image Processing, Universality Class, Dynamic Scaling Exponents, Fractals

15. NUMBER OF PAGES
13

16. PRICE CODE

17. SECURITY CLASSIFICATION OF REPORT	18. SECURITY CLASSIFICATION OF THIS PAGE	19. SECURITY CLASSIFICATION OF ABSTRACT	20. LIMITATION OF ABSTRACT
UNCLASSIFIED	UNCLASSIFIED	UNCLASSIFIED	UL

TABLE OF CONTENTS

LIST OF ILLUSTRATIONS

INTRODUCTION

Physical vapor deposition produces structures that are topologically and morphologically metastable (ref 1). Metal vapors condense into a fine-grained crystalline form on a chilled substrate, resulting in evolving structures that are inherently more disordered and less relaxed than those produced by other coating processes. The process control parameters determine the coarseness, shape, and distribution of these microstructures. These microstructural features affect the material properties and therefore the performance of a coating (ref 2). These features can be quantified in terms of self-affine scaling parameters (refs 3,4) that provide details on the intrinsic structure of the coating. Furthermore, the time evolution of these scaling parameters defines a unique *universality class* that is associated with the deposition process, and provides insight into the dynamics of the growth processes of thick metal films.

APPROACH

Sputtered niobium and tantalum coatings were prepared for analysis at various deposition stages using different substrates. Niobium was sputter deposited on silicon wafers, while tantalum was sputter deposited on silicon and stainless steel. The evolving coating morphology was characterized in terms of dynamic scaling exponents using atomic force microscopy (AFM) to map surface structures over a range of scales from 10-nm to 5-μm. The coating surface was assumed to be a homogenous, self-affine structure that is statistically invariant under anisotropic dilations for the AFM scan size employed in the measurements. Anisotropic scaling was measured in terms of the roughness exponent α, parallel correlation length $\xi_{//}(t)$, and the perpendicular correlation length $\xi_{\perp}(t)$. These scaling parameters provide information relating to the intrinsic properties of the surfaces over a range of scales after t minutes of sputtering. The anisotropic scaling described by α applies over a scaling range that is measured in terms of $\xi_{//}(t)$. The parallel correlation length is the distance beyond which there is no correlation in heights between points on the surface. The perpendicular correlation length, $\xi_{\perp}(t)$, characterizes fluctuations in the growth direction. It is related to the RMS surface roughness, $\sigma(t)$, by $\xi_{\perp}(t) = \sqrt{2} * \sigma(t)$. The values of α, $\xi_{//}(t)$, and $\xi_{\perp}(t)$ were determined using a generalized form of the height correlation function (ref 4)

$$C_h(\mathbf{r},t) = \langle [h(\mathbf{r}_0+\mathbf{r},\, t+t_0) - h(\mathbf{r}_0,t_0)]^2 \rangle_{t0,r0} \qquad (1)$$

where $h(\mathbf{r},t)$ is a single-valued height of the surface at location $\mathbf{r}$ at time t.

Correlations between points are time-dependent and generally increase with sputter time. Increasing grain size may be characterized by growth in the lateral ($\xi_{//}(t)$) direction by the *dynamic exponent* z. Corresponding changes in the growth direction are described by the *growth exponent*, β. In general, due to anisotropy of the deposition process, $\beta \neq z$. According to the dynamic scaling theory, at small sputter times, $\xi_{//}(t)$, and $\xi_{\perp}(t)$ are given by

$$\xi_{//} \propto t^{1/z} \qquad (2)$$

$$\xi_{\perp} \propto t^{\beta} \qquad (3)$$

The scaling exponents α, β, and z define a unique *universality class* that is independent of the details of the deposition process. They provide a unique metric for describing the evolving surface structure of the coating.

$C_h(r,t)$ is sensitive to dominant features of the substrate and variations in the curvature of the sample (ref 3). The influence of these effects can be minimized by analyzing the structure relative to a curved reference surface (refs 5,6) or by dividing the surface into patches that are analyzed separately using the "min-max" method (ref 7). Meisel (ref 5) suggests a technique for measuring scaling properties relative to a curved reference surface by limiting analysis to local, statistically homogenous regions that are large enough to define a statistically reliable $C_h(r,t)$. However, determining the size of local reference surfaces that properly adapt to the heterogeneity of the surface requires subjective investigator input. The "min-max" method (ref 7) requires the investigator to judge the number of local maxima and minima of the surface to use in the analysis.

Therefore, the time evolution of the coating surface was also characterized in terms of scaling exponents using detrended fluctuation analysis (DFA) (ref 8) to correct for inhomogeneities in the structure. Peng introduced DFA to determine long-term correlations embedded in time-series data. The sequence of integrated data of length N is divided into N/l nonoverlapping segments of length l. The average local variance of the segments is measured relative to a linear least-squares fit to the data within each segment l. The dependence of the variance on l defines the scaling properties of the time-series. In the present study, DFA was used to determine the scaling properties of surfaces in three-space using spatial averages of RMS variations for surface patches of width l measured relative to a plane-fit to the local data (Appendix A). The average variance is measured for geometrically increasing values of l ($l <$ system size L), and the dependence of the variance on l gives rise to the scaling properties of the fluctuations. The scaling properties are characterized by the roughness exponent α at time t

$$w_L(l,t) \sim l^{\alpha} \tag{4}$$

α is obtained from the scaling dependence of the local height variance, $w_L(l,t)$, on l, given by

$$w_L^2(l,t) \equiv \left\langle [h(\mathbf{r},t) - h_l(\mathbf{r},t)]^2 \right\rangle_{\mathbf{r}} \tag{5}$$

where $h(r,t)$ is the height of a single-valued surface at location r at time t relative to a plane-fit to the local data, $h_l(r,t)$ is the average local height at time t, t is the exposure time, and l is the size of local surface patches. A DFA is particularly useful for characterizing the unique structure of the coating, since the average local variance of the substrate can usually be subtracted from that of the coating. Figure 1 shows AFM data and the patchwork of local reference surfaces employed by DFA for l = 0.25, 0.5, and 1.0-μm. The system size (scan size) is L = 5-μm.

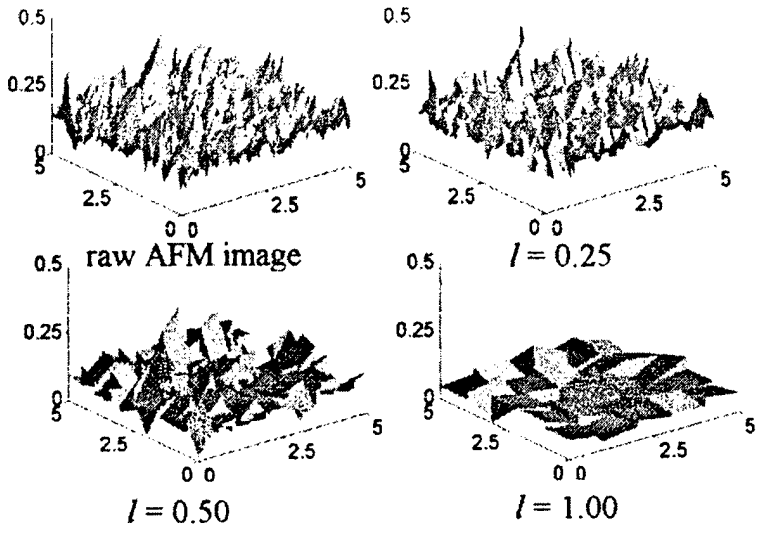

Figure 1. DFA reference patches for a 5-μm AFM image of sputtered niobium. (All dimensions in μm.)

Identifying the appropriate scaling region in the $C_h(r,t)$ or $w_L(l,t)$ data is critical in obtaining accurate estimates of the scaling parameters. The measured parameters depend on the range of data used to fit the linear region. Therefore, we developed a systematic procedure that determines them by fitting linear and polynomial splines to the height correlation results using the data that minimize the residuals in the fit (ref 9). We developed this technique since blind regression fits often result in incorrect values (ref 3). The linear range is determined by fitting a straight line, f_1, to the first k points and fitting a polynomial, f_2, to the remaining points in the set. k is the index of the data point at which the linear and curved segments meet. It is the variable knot (index) of a linear/curved spline and is a nonlinear parameter determined by exhaustion. The procedure is described in Appendix B.

RESULTS AND DISCUSSION

A series of tantalum and niobium sputtered silicon wafers was prepared for analysis at different stages using a rotating platform within a planar magnetron-sputtering chamber. The surface structure of 5 niobium coatings (15, 30, 45, 60, and 75 minutes of sputtering) and 4 tantalum coatings (15, 30, 60,and 120 minutes of sputtering) was characterized in terms of scaling exponents. Each sample had a unique, nonuniform morphology distribution across the surface. Therefore, the region with the greatest RMS variations in each specimen was used in the analysis. Simulations of the physical deposition process in our system do not predict the nonuniform coating distribution observed in the coatings (ref 10). However, they do predict variation in the angular distribution of the particles arriving at the surface. Therefore, the coating structure was analyzed at different locations across the sample to determine if α is a function of position due to particle shadowing. Figure 2 shows the variation in α and normalized $\xi_{\perp}(60)$ from the center to the edge of the sample for both sputtered tantalum and niobium. The figure shows the wide variation in RMS surface roughness ($\xi_{\perp}(t) = \sqrt{2} * \sigma(t)$) for both coatings. It also

illustrates that although α decreases monotonically for tantalum, it is insensitive to position for niobium. These results indicate that particle shadowing is not a significant effect and the monotonic decrease in α for tantalum can be associated with a phase transition from β-tantalum to α-tantalum across the sample (ref 10). This also indicates that α-tantalum develops an inherently more complex structure than β-tantalum.

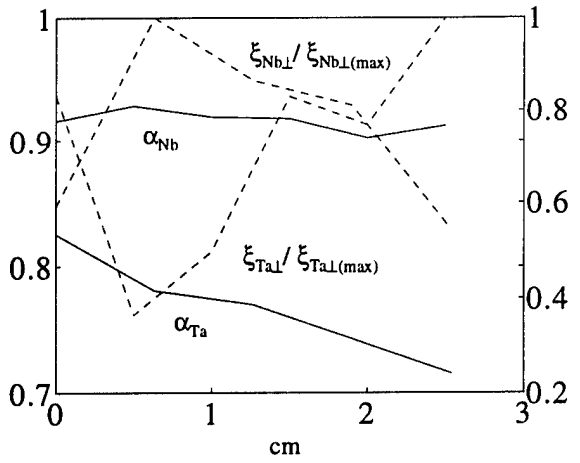

Figure 2. Roughness exponent (α) and normalized perpendicular correlation length ($\xi_{\perp}$)as a function of position on 60-minute sputtered samples of tantalum (Ta) and niobium(Nb).

The regions in each tantalum sample with the greatest RMS values correspond to the α-phase. Figure 3 shows AFM images of α-tantalum after 60 minutes and 120 minutes of sputtering. We were unable to identify a unique scaling region in $C_h(r,t)$ for these coatings (ref 10), as we did for the 15 to 45-minute sputtered tantalum coatings. This is likely a result of the evolution of the α-coating from a fine-grained microstructure into a material with large, complex grains. We were therefore unable to determine the dynamic scaling exponents for the evolving tantalum coating.

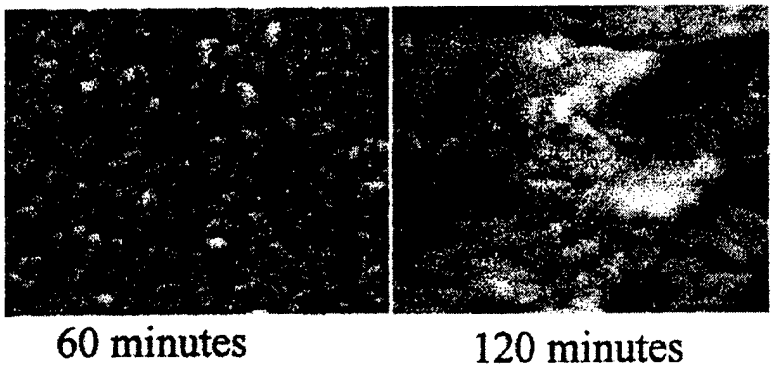

Figure 3. 5-μm scans of α-tantalum after 60 and 120 minutes of sputtering.

The microstructure of the sputtered niobium evolved differently from that of tantalum. Figure 4 shows the niobium coating after t = 15, 30, 60, and 75 minutes of sputtering, and Figure 5 shows the corresponding $C_h(r,t)$. The grain structure of the niobium coating is essentially Euclidian ($\alpha \geq 0.88$), with the grain size ($2^*\xi_{//}$) increasing from 188-nm to 368-nm. The values of grain size were validated with micrographs of the coatings. Figure 6 gives the time-dependence of $\xi_{//}(t)$ and $\xi_{\perp}(t)$, and shows that the evolving grain size and roughness is consistent with dynamic scaling theory. The value of β was determined to be 0.27, and $1/z = 0.31$ using all of the data for the fit. These results agree well with published results for sputtered deposited coatings (ref 11).

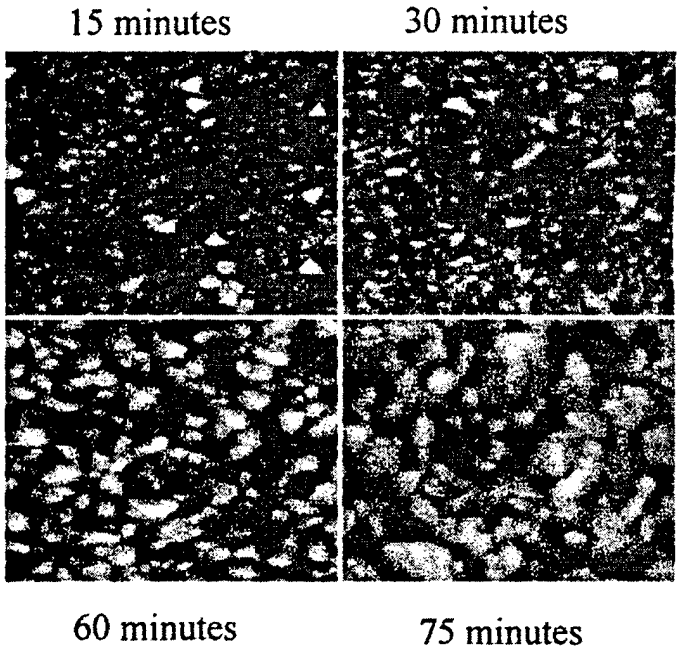

Figure 4. 5-μm scans of niobium after 15, 30, 60, and 75 minutes of sputtering.

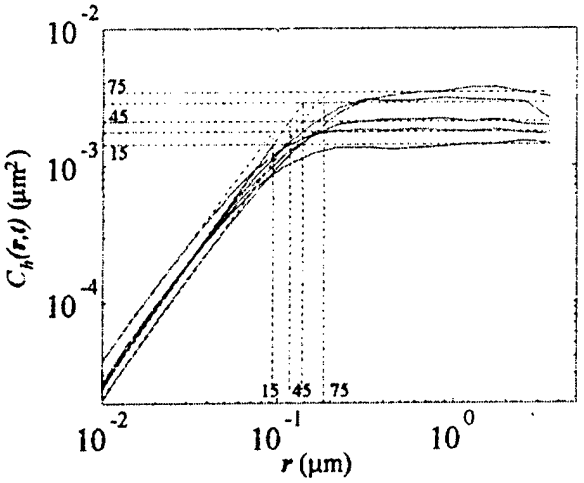

Figure 5. $C_h(r,t)$ for sputtered niobium with t = 15, 30, 45, 60, and 75 minutes.

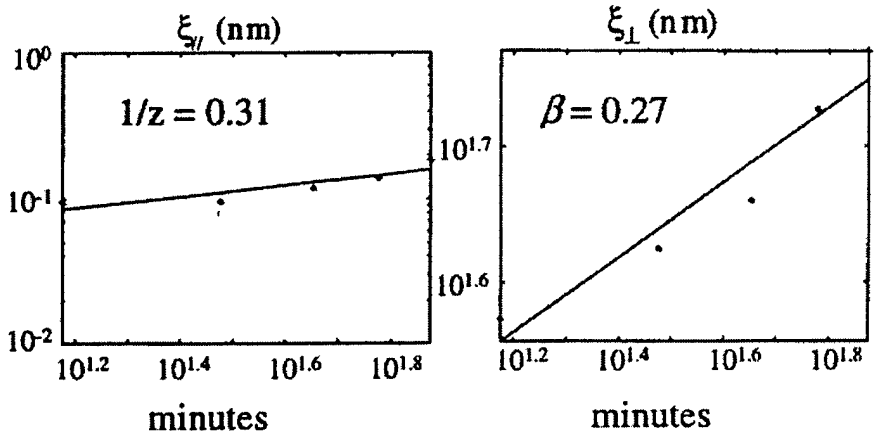

Figure 6. $\xi_{//}(t)$ and $\xi_{\perp}(t)$ for sputtered niobium.

The time evolution of sputtered niobium was also analyzed using DFA to identify long-range power-law correlations and correct for inhomogeneities in the surface structure. We have successfully tested DFA on model sets where the analytic solution is available and used DFA. We have also used DFA in the analysis of AFM images where there is localized curvature (ref 12). Figure 7 shows $C_h(r,t)$ and DFA results for a 60-minute sputtered niobium coating. The DFA results are scaled to match those of $C_h(r,t)$, since $|r| = l/2$, and at large r, $C_h(r,t) \rightarrow 2\sigma^2(t)$. The figure illustrates that DFA produces results that are inconsistent with those of $C_h(r,t)$. This occurs because DFA measures fluctuations about a plane-fit to local data and the niobium grains ($l < 2*\xi_{//}$) are essentially Euclidean (planar for $l << 2*\xi_{//}$). Figure 7 shows the breakdown of DFA for $l < 2*\xi_{//}$, at approximately 300-nm. Therefore, the dynamic scaling parameters of the niobium coating were also measured using fluctuation analysis. Fluctuation analysis determines the scaling properties of surfaces in three-space using spatial averages of RMS variations of

surface patches, but the RMS variations are not measured relative to a plane-fit to the local data. Figure 7 shows fluctuation analysis results scaled to match those of $C_h(r,t)$. The figure illustrates that appropriately scaled fluctuation analysis data return scaling parameters consistent with those of $C_h(r,t)$.

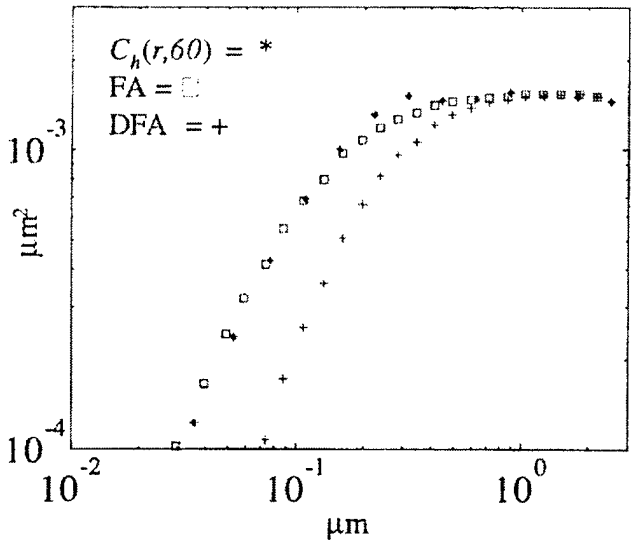

Figure 7. $C_h(r,60)$, scaled fluctuation analysis (FA), and DFA results for a niobium coating after 60 minutes of sputtering.

CONCLUSIONS

1. The structures of the coatings analyzed in this study are consistent with those of a self-affine surface fractal. However, the roughness and correlation lengths cannot always be described by single values across the range of scales.

2. Identifying the appropriate scaling region in $C_h(r,t)$ or $w_L(l,t)$ data is critical when measuring subtle changes in the scaling parameters of real data. Fitting linear and polynomial splines to $C_h(r,t)$ or $w_L(l,t)$ data provides a systematic approach for measuring the scaling parameters.

3. Scaling analysis indicates that the effect of particle shadowing on the intrinsic structure of the coatings produced in our sputtering system is minimal.

4. Detrended fluctuation analysis is a useful technique for measuring the scaling properties of a complex structure when there is inherent bias in the data. It is particularly valuable for characterizing the unique structure of a coating, since the average local variance of the substrate can usually be subtracted from that of the coating. However, DFA breaks down when measuring the scaling properties of Euclidean structures where variations about a planar (or higher order) fit to the data approach zero. In these cases, fluctuation analysis should be used.

5. The α–phase of tantalum is inherently more complex than the β–phase, and the time evolution of its microstructure cannot be described by a unique set of scaling parameters. However, the deposition of niobium is consistent with dynamic scaling theory, and the measured parameters provide a new metric for quantifying the evolving surface morphology.

REFERENCES

1. Turnbull, D., "Metastable Structures in Metallurgy," *Metallurgical Transactions A*, Vol. 12A, 1981, pp. 695-708.

2. Thornton, J.A., "The Microstructure of Sputter-Deposited Coatings," *Journal of Vacuum Science and Technology*, Vol. A4, No. 6, Nov/Dec 1986.

3. Barabasi A.L., and Stanley, H.E., *Fractal Concepts in Surface Growth*, Cambridge University Press, 1995.

4. Gouyet , J., Rosso, M., and Sapoval. B., *Fractals and Disordered Systems*, (A. Bunde and S. Havlin, Eds.), Springer, Berlin, 1991, pp. 229-234.

5 Meisel, L.V., Scanlon, R.D., Johnson, M.A., and Lanzerotti, Y.D., "Self-Affine Analysis on Curved Reference Surfaces: Self-Affine Fractal Characterization of a TNT Fracture Surface, *Shock Compression of Condensed Matter*, Vol. 1, 1999, pp. 727-730.

6. Cote, P.J., and Johnson, M.A., "Self-Affine Scaling Analysis of Coating Structure," *Proceedings of the SPIE Visual and Information Processing Conference*, Vol. 3716, 1999, pp. 2-8.

7. Peng, C.K., Buldyrev, S.V., Goldberger, A.L., Havlin, S., Sciortino, F., Simons, M., and Stanley, H.E., "Long-Range Correlations in Nucleotide Sequences, *Nature*, Vol. 356, 1992, pp. 168-171.

8. Peng, C.K., Buldyrev, S.V., Havlin, S., Simons, M., Stanley, H.E., and Goldberger, A.L., "Mosaic Organization of DNA Nucleotides," *Physical Review E*, Vol. 49, No. 2, 1994, pp. 1685-1688.

9. Johnson, M.A., "Measuring Dynamic Scaling Exponents in Evolving Structures," *Proceedings of the Systemics, Cybernetics, and Informatics Conference*, Vol. 5, 2000, pp. 112-116.

10. Johnson M.A., and Cote, P.J., "Characterization of Metastable Structures in Sputtered Coatings, *Proceedings of the Systemics, Cybernetics, and Informatics Conference*, Vol. 6, 2001, pp. 298-303.

11. Miller, D.J., Gray, K.E., Kampwirth, R.T., and Murduck, J.M., "Studies of Growth Instabilities and Roughening in Sputtered NbN Films Using a Multilayer Decoration Technique, *Europhysics Letters*, Vol. 19, 1992, pp. 27-32.

12. Johnson, M.A., and Cote, P.J., "Detrended Fluctuation Analysis of UV Degradation in a Polyurethane Coating," submitted to *Journal of Coatings Technology*, to be published.

APPENDIX A

The following series of equations provides the coefficients of a plane-fit ($f(x,y) = a + bx + cy$) to the data z_i that minimize the square of the residuals $(\varepsilon_i = a + bx_i + cy_i - z_i)^2$ for all points, m, containing a local surface patch of length l:

$$\frac{\partial S}{\partial a} = 0 \Rightarrow a * m + b\sum_{1}^{m} x_i + c\sum_{1}^{m} y_i = \sum_{1}^{m} z_i \tag{A1}$$

$$\frac{\partial S}{\partial b} = 0 \Rightarrow a\sum_{1}^{m} x_i + b\sum_{1}^{m} x_i^2 + c\sum_{1}^{m} x_i y_i = \sum_{1}^{m} x_i z_i \tag{A2}$$

$$\frac{\partial S}{\partial c} = 0 \Rightarrow a\sum_{1}^{m} y_i + b\sum_{1}^{m} x_i\, y_i + c\sum_{1}^{m} y_i^2 = \sum_{1}^{m} y_i z_i \tag{A3}$$

APPENDIX B

This procedure was developed to determine if a scaling region exists and to determine estimates of the scaling region. It measures the geometric parameters by fitting linear and polynomial splines to $C_h(\boldsymbol{r},t)$ or $w_L(l,t)$ data, and estimating the values of $\xi_{/\!/}$ and α using the data that minimize the residuals in the fit. The linear range is determined by the fitting a straight line, f_1, to the first k points and fitting a polynomial, f_2, to the remaining points in the set, k through m. k is the index of the data point at which the linear and curved segments meet. It is the variable knot (index) of a linear/curved spline and is a nonlinear parameter determined by exhaustion. The coefficients of the polynomials are evaluated with continuity enforced at k, and the residuals (ε_i) are computed over the entire range. The value of k, for which the residuals are a minimum, is selected as the index for the last point of the linear range. k is computed using a quadratic, cubic, and quartic for f_2. C^1 and C^2 continuity are enforced for the quartic fit. C^2 continuity is not enforced for the cubic fit to allow some overshoot in the data. The largest of the three values of k is used to ensure that the maximum number of points in the linear region is selected to determine α. If k is less than three, it is assumed no linear region exists and the system does not adhere to fractal theory. $\xi_{/\!/}$ is then determined from the intersection of the linear fit and $\xi_{\perp}$. The points used to compute $\xi_{\perp}$ are at large $\boldsymbol{r}$ where no correlation is observed. The procedure for the quartic, cubic, and quadratic fits is described in detail in Reference 9. The procedure for the quartic fit is repeated below as

$$f_1(x) = a + b(x-k) \tag{B1}$$

$$f_2(x) = c + d(x-k) + e(x-k)^2 + f(x-k)^3 + g(x-k)^4 \tag{B2}$$

For C^2 continuity at knot k,

$$f_1(k) = f_2(k);\ f_1'(k) = f_2'(k);\ f_1''(k) = f_2''(k) \tag{B3}$$

and the residuals (ε_i) become

$$\varepsilon_i = a + b\,p_i - y_i \quad for\ i \le i_k$$

$$\varepsilon_i = a + b\,p_i + f\,q_i + g\,r_i - y_i \quad for\ i > i_k$$

where

$$p_i = x_i - k;\ q_i = (x_i - k)^3;\ r_i = (x_i - k)^4 \tag{B4}$$

Minimizing the sum of the squares of the residuals S

$$S = \sum_{i=0}^{m} \varepsilon_i^2 = \sum_{LR} \varepsilon_i^2 = \sum_{i=0}^{i_k} \varepsilon_i^2 + \sum_{i=i_{k+1}}^{m} \varepsilon_i^2 = \sum_{L} \varepsilon_i^2 + \sum_{R} \varepsilon_i^2 \tag{B5}$$

$$\frac{\partial S}{\partial a} = 0 \Rightarrow a * m + b \sum_{LR} p_i + f \sum_{R} q_i + g \sum_{R} r_i = \sum_{LR} y_i \tag{B6}$$

$$\frac{\partial S}{\partial b} = 0 \Rightarrow a \sum_{LR} p_i + b \sum_{LR} p_i^2 + f \sum_{R} p_i q_i + g \sum_{R} p_i r_i = \sum_{LR} p_i y_i \tag{B7}$$

$$\frac{\partial S}{\partial g} = 0 \Rightarrow a \sum_{R} r_i + b \sum_{R} p_i r_i + f \sum_{R} q_i r_i + g \sum_{R} r_i^2 = \sum_{R} r_i y_i \tag{B8}$$

$$\frac{\partial S}{\partial f} = 0 \Rightarrow a \sum_{R} q_i + b \sum_{R} p_i q_i + f \sum_{R} q_i^2 + g \sum_{R} q_i r_i = \sum_{R} q_i y_i \tag{B9}$$

The systems of equations (B6) through (B9) are solved for coefficients a, b, f, and g for k ranging from 2 to m-1. The data point corresponding to the value of k, for which residuals are a minimum, is used as the last point in the linear fit. $\xi_{//}$ is then determined from the intersection of the linear fit and $\xi_{\perp}$.

TECHNICAL REPORT INTERNAL DISTRIBUTION LIST

	NO. OF COPIES
TECHNICAL LIBRARY ATTN: AMSTA-AR-CCB-O	5
TECHNICAL PUBLICATIONS & EDITING SECTION ATTN: AMSTA-AR-CCB-O	3
OPERATIONS DIRECTORATE ATTN: SIOWV-ODP-P	1
DIRECTOR, PROCUREMENT & CONTRACTING DIRECTORATE ATTN: SIOWV-PP	1
DIRECTOR, PRODUCT ASSURANCE & TEST DIRECTORATE ATTN: SIOWV-QA	1

NOTE: PLEASE NOTIFY DIRECTOR, BENÉT LABORATORIES, ATTN: AMSTA-AR-CCB-O OF ADDRESS CHANGES.

TECHNICAL REPORT EXTERNAL DISTRIBUTION LIST

	NO. OF COPIES
DEFENSE TECHNICAL INFO CENTER ATTN: DTIC-OCA (ACQUISITIONS) 8725 JOHN J. KINGMAN ROAD STE 0944 FT. BELVOIR, VA 22060-6218	2
COMMANDER U.S. ARMY ARDEC ATTN: AMSTA-AR-WEE, BLDG. 3022 AMSTA-AR-AET-O, BLDG. 183 AMSTA-AR-FSA, BLDG. 61 AMSTA-AR-FSX AMSTA-AR-FSA-M, BLDG. 61 SO AMSTA-AR-WEL-TL, BLDG. 59 PICATINNY ARSENAL, NJ 07806-5000	 1 1 1 1 1 2
DIRECTOR U.S. ARMY RESEARCH LABORATORY ATTN: AMSRL-DD-T, BLDG. 305 ABERDEEN PROVING GROUND, MD 21005-5066	 1
DIRECTOR U.S. ARMY RESEARCH LABORATORY ATTN: AMSRL-WM-MB (DR. B. BURNS) ABERDEEN PROVING GROUND, MD 21005-5066	 1
COMMANDER U.S. ARMY RESEARCH OFFICE ATTN: TECHNICAL LIBRARIAN P.O. BOX 12211 4300 S. MIAMI BOULEVARD RESEARCH TRIANGLE PARK, NC 27709-2211	 1

	NO. OF COPIES
COMMANDER ROCK ISLAND ARSENAL ATTN: SIORI-SEM-L ROCK ISLAND, IL 61299-5001	 1
COMMANDER U.S. ARMY TANK-AUTMV R&D COMMAND ATTN: AMSTA-DDL (TECH LIBRARY) WARREN, MI 48397-5000	 1
COMMANDER U.S. MILITARY ACADEMY ATTN: DEPT OF CIVIL & MECH ENGR WEST POINT, NY 10966-1792	 1
U.S. ARMY AVIATION AND MISSILE COM REDSTONE SCIENTIFIC INFO CENTER ATTN: AMSAM-RD-OB-R (DOCUMENTS) REDSTONE ARSENAL, AL 35898-5000	 2
COMMANDER U.S. ARMY FOREIGN SCI & TECH CENTER ATTN: DRXST-SD 220 7TH STREET, N.E. CHARLOTTESVILLE, VA 22901	 1

NOTE: PLEASE NOTIFY COMMANDER, ARMAMENT RESEARCH, DEVELOPMENT, AND ENGINEERING CENTER, BENÉT LABORATORIES, CCAC, U.S. ARMY TANK-AUTOMOTIVE AND ARMAMENTS COMMAND, AMSTA-AR-CCB-O, WATERVLIET, NY 12189-4050 OF ADDRESS CHANGES.